Original Article

Breast Cancer Subtype Prediction Model Employing Artificial Neural Network and ^{18}F-Fluorodeoxyglucose Positron Emission Tomography/ Computed Tomography

Alamgir Hossain, Shariful Islam Chowdhury[1]

Department of Physics, University of Rajshahi, Rajshahi-6205, [1]Institute of Nuclear Medicine and Allied Sciences, Bangladesh Atomic Energy Commission, Rajshahi, Bangladesh

Abstract

Introduction: Although positron emission tomography/computed tomography (PET/CT) is a common tool for measuring breast cancer (BC), subtypes are not automatically classified by it. Therefore, the purpose of this research is to use an artificial neural network (ANN) to evaluate the clinical subtypes of BC based on the value of the tumor marker. **Materials and Methods:** In our nuclear medical facility, 122 BC patients (training and testing) had ^{18}F-fluoro-D-glucose (^{18}F-FDG) PET/CT to identify the various subtypes of the disease. ^{18}F-FDG-18 injections were administered to the patients before the scanning process. We carried out the scan according to protocol. Based on the tumor marker value, the ANN's output layer uses the Softmax function with cross-entropy loss to detect different subtypes of BC. **Results:** With an accuracy of 95.77%, the result illustrates the ANN model for K-fold cross-validation. The mean values of specificity and sensitivity were 0.955 and 0.958, respectively. The area under the curve on average was 0.985. **Conclusion:** Subtypes of BC may be categorized using the suggested approach. The PET/CT may be updated to diagnose BC subtypes using the appropriate tumor maker value when the suggested model is clinically implemented.

Keywords: ^{18}F-fluoro-D-glucose positron emission tomography/computed tomography, artificial neural network, breast cancer, histological subtypes, prediction model

Received on: 25-12-2023 **Review completed on: 17-03-2024** **Accepted on: 14-04-2024** **Published on: 25-06-2024**

Introduction

Breast cancer (BC) is one of the most severe and frightening diseases that strike women of all ages, impacting one in every three women with the condition and having the second-highest death rate after skin cancers.[1] It is common knowledge that BCs only occur in women, yet male BC is uncommon but not unheard of, accounting for 1% of all cancer diagnoses in males globally.[2] Even though women over 50 are more likely to have BC, people under 40 can also acquire it.[3] Young patients are uncommon in affluent nations, but in areas such as Africa and the Middle East, the rate of young BC patients can approach 20%, which is relatively high.[4] The etiology of BC can be hereditary or environmental, and these variables contribute to the onset and recurrence of this potentially fatal disease.[5] While proper diagnosis and early therapy can cure BC, 30% of patients have a 10-year survival rate.[6] BC can take many different forms. Ductal carcinoma is a noninvasive or preinvasive form of BC that begins in the milk dust and does not move to the surrounding breast tissue. Invasive lobular cancer (ILC) and invasive ductal cancer (IDC) are the two types of invasive BC. Other specific forms of BC include angiosarcoma, phyllodes tumor, Paget's disease of the breast, inflammatory BC, and triple-negative BC.[7] ILC is BC that is the second most invasive, contributing to 5%–15% of BC.[8-11] This cancer is hormonally estrogen and progesterone receptor. The receptor is positive estrogen receptor (ER)/progesterone receptor and negative human epidermal growth factor receptor 2 (HER2).[12,13] These tumors are ill-defined margins with larger shapes[13,14] and metastatic patterns with gastrointestinal and peritoneal site movement.[15-17]

Access this article online

Quick Response Code:

Website: www.jmp.org.in

DOI: 10.4103/jmp.jmp_181_23

Address for correspondence: Dr. Alamgir Hossain, Department of Physics, University of Rajshahi, Rajshahi 6205, Bangladesh. E-mail: alamgir_ru07@yahoo.com

How to cite this article: Hossain A, Chowdhury SI. Breast cancer subtype prediction model employing artificial neural network and ^{18}F-fluorodeoxyglucose positron emission tomography/ computed tomography. J Med Phys 2024;49:181-8.

The spread of cancer through the lymphovascular system, histologic grade, the condition of specific hormone receptors, overexpression of ERBB2 (HER2 or HER2/neu), and the patient's menopausal status are all critical variables in the prognosis of BC, and therapy varies depending on these aspects.[18] The stage at which metastases in lymph nodes (LNs) originated is also an essential determinant, with axillary nodal metastases being the most relevant for prognostic reasons.[6,18] The most important factor for better treatment and a higher survival rate is early detection of the malignancy inside the patient's body, which can be accomplished by performing a variety of medical tests and techniques on the patients, such as nuclear imaging, mammography, biopsy, ultrasound, and so on.[19]

The size and grade of the tumor, the patient's endocrine (hormonal) receptor (ER) and HER2 status, the involvement of the axillary LNs, and metastatic dissemination are among the factors that affect BC therapy and prognoses. The degree of axillary LN metastasis is thought to be the most accurate indicator of BC survival among these variables.[20] Determining the patient's axillary nodal status before therapy is important since it can influence management choices. Sentinel LN biopsy, axillary LN dissection, and pathological evaluation of aspiration cytology are considered the "gold standard" for identifying axillary LN involvement; yet, these are invasive techniques. On the other hand, various research groups[21-25] have described the usefulness of noninvasive 2-deoxy-2-^{18}F-fluoro-D-glucose positron emission tomography/computed tomography (2-^{18}F-FDG-PET/CT) for the diagnosis of axillary LN metastasis in patients with BC. One of these groups was able to achieve a relatively low pooled sensitivity value of 60% and a very high pooled specificity value of 97%.[26] Recent artificial intelligence (AI) technologies are worth considering to help doctors employing 2-^{18}F-FDG-PET/CT diagnose axillary LN metastases more accurately. Medical image analysis has made extensive use of deep-learning methods, which are based on deep convolutional neural networks,[27] such as 2-^{18}F-FDG-PET/CT.[28]

^{18}F-FDG PET/CT may be the essential tool for the early identification of stage III BC.[29] It is the instrument for detecting the sensitivity and specificity of breast carcinoma as recurrent.[30] It is also the baseline for diagnosis, prognosis, and treatment for BC with optimal nodal staging.[31,32] It provided false-positive findings for malignancies or benign.[33] The malignant or synchronous tumor was detected for lesion detection using ^{18}F-FDG PET/CT.[34,35] Based on ^{18}F-FDG PET/CT, an artificial neural network (ANN) was employed for predicting pulmonary lesions[36] and head-and-neck cancer.[37] A deep learning model was also used to detect LNs of lung cancer using ^{18}F-FDG PET/CT.[38]

ANN may also be employed to differentiate between benign and malignant tumors based on the quantity of FDG absorption by tumor cells in a PET/CT. This software may be used to pinpoint a breast tumor's precise location, whether it is malignant or not, and how much it has spread around the area since it employs features based on neural connections and can readily turn a set of detailed data into a simple output. ANN application in nuclear imaging with ^{18}F-FDG PET/CT for BC allows for the precise identification of malignant cells, which aids in the diagnosis of BC and optimal treatment planning with accuracy. As a result, the aim of this work is to evaluate the clinical subtypes of BC based on an ANN on the value of tumor markers.

Materials and Methods

One hundred and forty-two patients participated in the study, including training and testing with K-fold cross-validation. The Institutional Review Board authorized the requirement for formal IRB approval, and the parents provided written informed consent for the scientific use of the data. There were no significant differences for patient characteristics. The characteristics are given in Table 1. Table 1 shows the mean age, height, weight, blood glucose, injected amount of ^{18}F-FDG, and tumor marker. Table 1 also demonstrates the histological subtypes, including IDC, ILC, and other subtypes. The whole procedure is shown in Figure 1. Table 1 shows the baseline for patients, including age, height, weight, blood glucose, injected amount of ^{18}F-FDG, tumor maker, and histological subtypes. The median age, size, weight, blood glucose, injected amount of ^{18}F-FDG, and tumor markers are 50 (26–73) years, 151 (134–170) cm, 64 (35–148) kg, 6 (3.6–12.4) mmol/L, 4.97 (2.89–8.84) mCi, and 21.35 (1.3–283) U/ml, respectively. The histological subtypes are IDC (119), ILC (14), and others (9). Table 2 indicates the case processing summary for the ANN, including 142 samples (training: 98, testing:

Table 1: Baseline characteristics for patients

Characteristics	Median (range, minimum–maximum)	Histological subtypes		
		IDC	ILC	Others
Age (years)	50 (26–73)	119	14	9
Height (cm)	151 (134–170)			
Weight (kg)	64 (35–148)			
Blood glucose (mmol/L)	6 (3.6–12.4)			
Injected amount of ^{18}F-FDG (mCi)	4.97 (2.89–8.84)			
Tumor marker (CA-15-3, U/mL)	21.35 (1.3–283)			

ILC: Invasive lobular cancer, IDC: Invasive ductal cancer, ^{18}F-FDG: ^{18}F-fluorodeoxyglucose

44), where 69.0% for the training dataset and 31.0% for the testing dataset.

Before the PET/CT scans with ^{18}F-FDG, every patient had fasted for a minimum of 6 h. One hour before to PET/CT scans, 4.07 MBq/kg of ^{18}F-FDG was intravenously given once a blood glucose level of <150 mg/dL was confirmed. Using a specialized PET/CT scanner, all ^{18}F-FDG scans were carried out in a supine posture from the base of the cranium to the proximal thigh (Philips Healthcare, Cleveland, OH, USA). For attenuation correction and anatomical data, a CT scan with no contrast enhancement was carried out at 100 mA and 120 kVp. Using three-dimensional acquisition mode, a PET scan was conducted for 5–7 positions for 1½ min each bed position. Using time-of-flight reconstruction and point-spread-function modeling, PET images were reconstructed with attenuation correction (2 iterations and 21 subsets). All PET/CT quantitative analyses were carried out by two nuclear medicine doctors with 5 and 12 years of expertise in PET/CT imaging, respectively. Every ^{18}F-fluoride PET/CT picture was quantitatively evaluated to identify BC. PET/CT picture quantification was done using Metavol® software.[39] The maximal standardized uptake value for primary BC was ascertained. Figure 2 shows BC.

Table 2: Summary for cases to build up the artificial neural network model

Case processing summary	
Sample	***n* (%)**
Training	98 (69.0)
Testing	44 (31.0)
Total	142 (100.0)

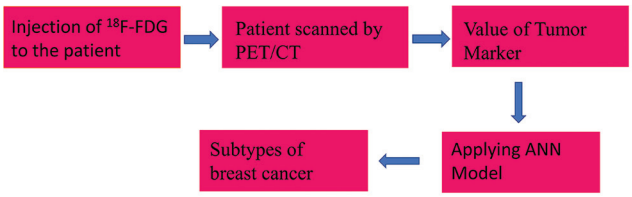

Figure 1: The illustration for estimating histological subtypes for breast cancer using an artificial neural network based on the value of the tumor maker. ^{18}F-FDG: ^{18}F-fluoro-D-glucose, PET/CT: Positron emission tomography/computed tomography, ANN: Artificial neural network

ANN model is described in Figure 3. Three layers make up the model: input, hidden, and output. The input and output layers are linked to the neurons. The input layer included age, height, weight, blood glucose, injection amount, and tumor marker. To minimize the loss function, the output layers employed the Softmax activation function with cross-entropy. The label of the output layer was IDC, ILC, and other subtypes. The model was specified with synaptic weight >0 and synaptic weight <0. The values of the learning rate, momentum, interval offset, and interval center were, in order, 0.4, 0, 0.9, and 0.5. The epoch had a maximum value of 100. K-fold cross-validation was used to divide the data into training and testing sets. The loss function, which is cross-entropy loss, is described below:

The cross-entropy:

$$1 = -\sum_{i=j}^{m} y_i \log\left(p_i\right) \quad (1)$$

where l defines the loss and $y_i \in \{0,1\}$ describes the category. To determine the prediction confidence p_i, m denotes the number of types.[40,41]

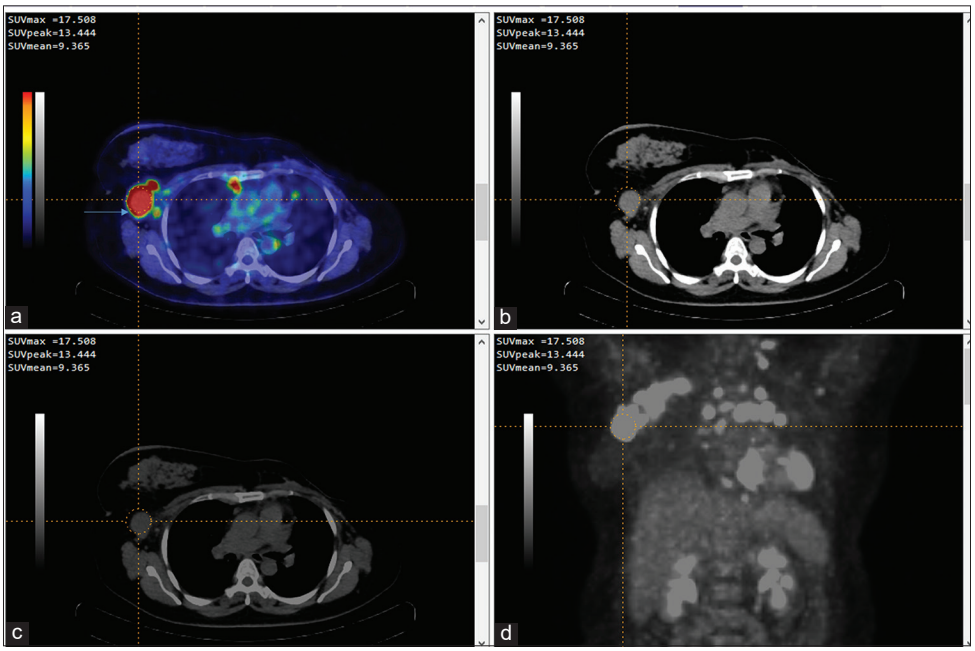

Figure 2: ^{18}F-fluorodeoxyglucose positron emission tomography/computed tomography for breast cancer. (a) PET/CT fusion image (axial section). The blue arrow indicates breast cancer (upper left). (b) CT image in Axial section (Upper Right). (c) PET image in Axial Section (lower left). (d) PET image in coronal section (Lower Right)

The Softmax function is:

$$P_i = \frac{e^{x_i}}{\sum_{j=1} e^{x_i}} \quad (2)$$

where x_i is the feature for the i_{th} category. The Softmax activation function can be distributed for the normalized categorical distribution. The highest value is highlighted, and other matters are super impressed due to the exponential function.[41,42]

The output value for IDC, ILC, and other subtypes is shown in Supplementary Figures 1-3, respectively. The Softmax activation function provides discounts between 0 and 1, and the sum will be 1. It will maintain the order, rank, and sequence. Nearly 1 will have the highest likelihood, and 0 will have the lowest possibility. The desired and model output is in the following:

IDC, for instance, is the input. The logits for the quantity of injected activity were 7.39 mCi, 5.56 mCi, and 3.45 mCi, in that order. We discovered that the output probabilities are 0.85, 0.13, and 0.02, respectively, using the Softmax activation function in the output layer. The intended output for Class IDC is (1, 0, 0), which we quantify using the cross-entropy; nevertheless, Supplementary Figure 1 shows that the model output is (0.85, 0.13, 0.02).

ILC, for instance, is the input. Similarly, the logits for the quantity of injected activity were 7.39 mCi, 5.56 mCi, and 3.45 mCi, correspondingly. We determined the output probabilities to be 0.85, 0.13, and 0.02, respectively, using the Softmax activation function in the output layer. For Class ILC, we measure the desired output (0, 1, 0) using the cross-entropy; however, Supplementary Figure 2 shows that the model output is (0.85, 0.13, 0.02).

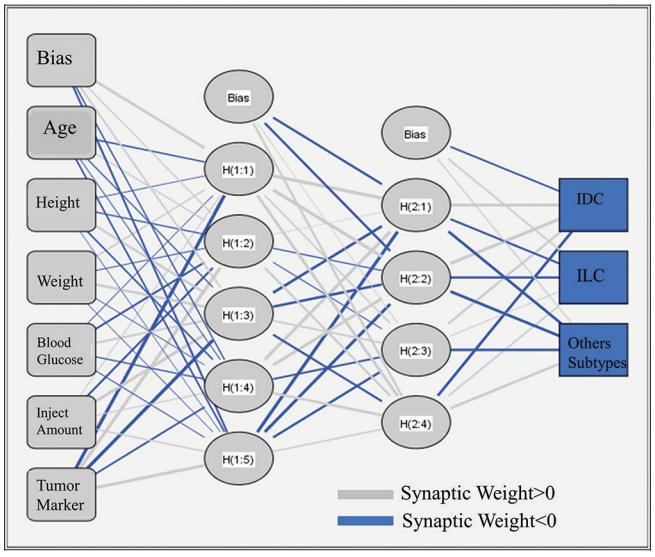

Figure 3: Artificial neural networks for obtaining subtypes (invasive ductal cancer, invasive lobular cancer, and others) used the sigmoid function as a hidden layer and output layer with the Softmax function. ILC: Invasive lobular cancer, IDC: Invasive ductal cancer

Other subtypes are an example of the input. Similarly, the logits for the quantity of injected activity were 7.39 mCi, 5.56 mCi, and 3.45 mCi, correspondingly. The output probabilities that resulted from using the Softmax activation function in the output layer were 0.85, 0.13, and 0.02, in that order. For the other subtypes, we measured the intended output {0,0,1} using the cross entropy; however, Supplementary Figure 3 shows that the model output is (0.85, 0.13, 0.02).

The Transport Reporting of Multivariable Prediction Model for Individual Prognosis Or Diagnosis indicates that[43] there is no recommended random selection for the prediction model for training and validation data for minor cases. The input feature for preprocessing was normalized. Using the original search engine, Wrapper was the subset evaluator that was applied to obtain the best feature section for the model of subtypes for BC through Waikato Environment for Knowledge Analysis.

Statistical techniques

An ANN system was created using IBM Crop., Armonk, New York, USA's SPSS software (Version 21.0). GraphPad Prism 8 was used for the attributes of tumor subtypes. *P* values were deemed statistically significant if they were < 0.05.

Results

Table 3 shows the ANN models, including input, hidden, and output layers. The out layer provided the subtypes such as IDC, ILC, and other subtypes using cross-entropy function with Softmax activation function [Figure 3]. Figure 3 indicates the significant level for the attributes of BC subtypes (a) IDC, (b)

Table 3: Details of the parameters for the input, hidden, and output layers

Network information	
Input layer	
Covariates	
1	Age
2	Height (cm)
3	Weight (kg)
4	Blood glucose
5	Injected amount
6	Tumor marker
Number of units[a]	6
Rescaling method for covariates	Standardized
Hidden layer (s)	
Number of hidden layers	2
Number of units in hidden layer 1[a]	5
Number of units in hidden layer 2[a]	4
Activation function	Sigmoid
Output layer	
Dependent variables	
1	Class
Number of units	3
Activation function	Softmax
Error function	Cross-entropy

[a]Excluding the bias unit

ILC, and (c) others. The attributes of blood glucose and injected amount are nonsignificant to each other. In contrast, the attributes of tumor marker is significant with blood glucose and injected amount for subtypes IDC, ILC, and others, respectively [Figure 4].

Table 4 demonstrates the confusion matrix for the ANN model of BC subtypes. The diagonal element indicates the number of correct subtypes for IDC (119), ILC (10), and others (7), and also the no diagonal part present for the noncorrect number of subtypes, respectively, to count the accuracy of the model. The ANN model with an accuracy of 95.77% for K-fold cross-validation is shown in Supplementary Table 1. The corresponding averages for specificity and sensitivity were 0.889 and 0.958. The area under the curve (AUC) on average was 0.985. Figure 4 describes the attributes of the subtypes of the tumor. The tumor marker was higher than all other attributes where the injected amount was lower. Figure 5 indicates the receiver operating characteristic curve, demonstrating that the AUC values are 0.9872, 0.9637, and 0.995 for IDC, ILC, and other subtypes, respectively.

Discussion

The use of ^{18}F-FDG PET/CT for prognostic and therapeutic purposes has been demonstrated for early BC diagnosis.[44-46] Groheux *et al*.[47] demonstrated the subtypes of BC for early detection based on the pathology response. Usmani *et al*.[48]

Table 4: Confusion matrix used artificial neural network for obtaining subtypes

Confusion matrix			
a	**b**	**c**	**Classified as**
119	0	0	a=IDC
3	10	1	b=ILC
0	2	7	c=Others

ILC: Invasive lobular cancer, IDC: Invasive ductal cancer

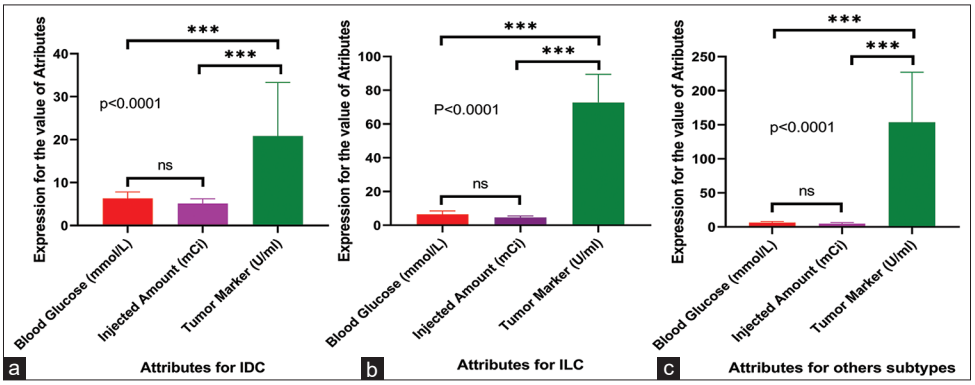

Figure 4: (a) The expression for the value of attributes for invasive ductal cancer, (b) The expression for the value of attributes for invasive lobular cancer, and (c) The expression for the value of attributes for other subtypes. The significance ($P < 0.05$) is indicated by the asterisk. ILC: Invasive lobular cancer, IDC: Invasive ductal cancer

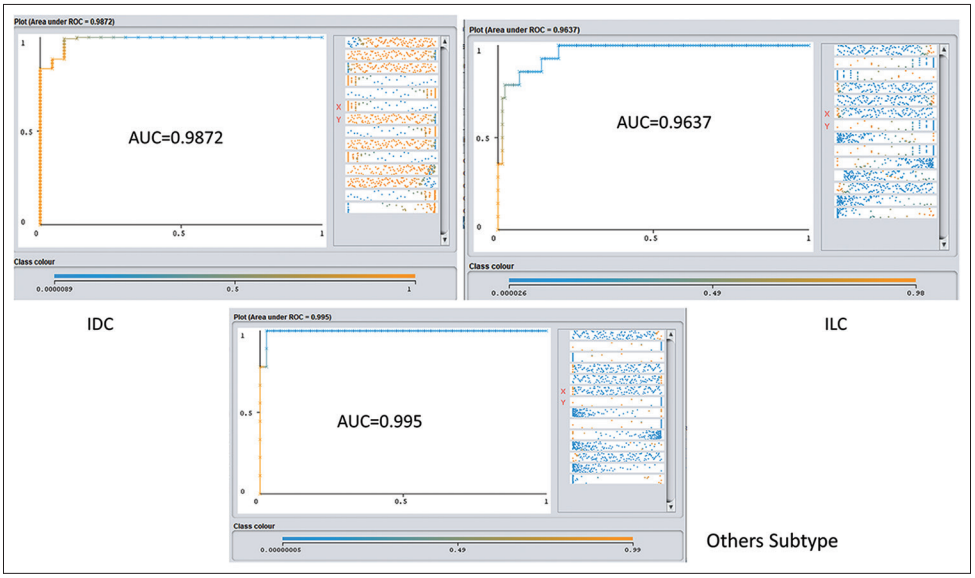

Figure 5: The receiver operating characteristic curve for invasive ductal cancer, invasive lobular cancer, and other subtypes of breast cancer. AUC: Area under the curve, ILC: Invasive lobular cancer, IDC: Invasive ductal cancer

find out the evaluation and answer of breast lymphoma. Taralli *et al*.[49] proposed that good outcomes were obtained when an ANN was used to predict nodal involvement in nonsmall cell lung cancer preoperatively using ^{18}F-FDG-PT/CT. Luo *et al*.[36] suggested an ANN model for solitary pulmonary lesions, demonstrating the AUC was 83.3%, 86.7%, and 86.0% for three models that indicated the ability of the model to measure the improvement of diagnostic accuracy. The accuracy measurement for BC diagnosis demonstrating an AI-based deep learning model was widespread and included ^{18}F-FDG-PET/CT.[27,28] Li *et al*.[50] showed that the AI-based deep learning model to evaluate the LN metastasis using the improvements in accuracy, sensitivity, and specificity with ^{18}F-FDG PET/CT was 64.2%, 99.5%, and 0.5%, respectively. Inaki *et al*.[51] provided an ANN model for the diagnosis of bone scan index for BC patients using ^{18}F-FDG PET/CT. Lung, breast, head-and-neck, and cervical cancers may all be detected and diagnosed with AI. Machine learning can differentiate tumors, segmentation, staging, and assessment response, but the routine-based AI for cancer diagnosis with radiomics is limited.

A pilot study has been conducted to identify tissue signatures with sensitivity and specificity using ^{18}F-FD in PT/CT, demonstrating that AI can recognize the lesion of breast cancer based on deep learning.[52] Li *et al*.[50] proposed an AI-based model for diagnosing using ^{18}F-FDG-PT/CT for axillary LN metastasis in BC, describing a sensitivity of 64.2% and specificity of 99.5% where the clinical result was better than the result of AI-based diagnosis. Still, AI belongs to a positive impact on the accuracy of diagnosis.

Dihge *et al*.[53] proposed an ANN model for predicting nodal status for BC. Sepandi *et al*.[54] suggested an AAN model for the recommendation of predictive biopsy value for assessment of the diagnosis, exhibiting an AUC of 0.955, sensitivity of 0.82, and specificity of 0.90. A model was proposed for ANN based on ultrasound imaging in BC, described with an accuracy of 92.4%.[55]

Early cancer detection has been focused on the literate based on the ANN model with image processing.[56] A deep learning model for BC was proposed by Jia *et al*.; it showed an AUC of 0.99, sensitivity of 96.32%, and specificity of 89.59%.[57] Ren *et al*. presented a CNN-based model that uses ^{18}F-FDG-PET/CT to detect BC metastasis for T1-W magnetic resonance imaging (MRI), T2-W MRI, dynamic contrast-enhanced MRI, T1-W + T2W MRI, and dynamic contrast-enhanced DECE-T2-W MRI. They showed that the accuracy ranged from 86.08% to 88.50% and the AUC was between 0.804 and 0.882.[58] In our study, the ANN model yielded a sensitivity of 0.958 and a specificity of 0.889, respectively. Its AUC was 0.985. The AUC values were 0.9872, 0.9637, and 0.985 for IDC, ILC, and other subtypes.

In spite of the success of this research, some things could be improved. First, we need to follow up with the patients. We use only data from our institute, not other institutes. It needs to check data from other institutions for diversity. Second, the sample size was small. Third, it is difficult to go into detail about the integration and relationship between the unknown variables even if the accuracy was higher. Finally, our proposed model and clinicians' merit would be considered to be practiced clinically if we investigate a large dataset with other machine learning models.

Conclusion

This conclusion is supported by the research's findings and the information at hand. For training and testing, the accuracy, sensitivity, and specificity were better. The suggested method can identify if a breast tumor belongs to the IDC, ILC, or another subtype. After the recommended method is put into practice clinically, it might build an ^{18}F-FDG PET/CT to identify the subtypes based on the characteristics of the tumor using the ANN model.

Acknowledgment

We are acknowledged for providing data from the Institute of Nuclear Medical Physics, Saver, Bangladesh Atomic Energy Commission, Bangladesh.

Financial support and sponsorship

Nil.

Conflicts of interest

There are no conflicts of interest.

References

1. DeSantis C, Siegel R, Bandi P, Jemal A. Breast cancer statistics, 2011. CA Cancer J Clin 2011;61:409-18.
2. Gucalp A, Traina TA, Eisner JR, Parker JS, Selitsky SR, Park BH, *et al.* Male breast cancer: A disease distinct from female breast cancer. Breast Cancer Res Treat 2019;173:37-48.
3. Radecka B, Litwiniuk M. Breast cancer in young women. Ginekol Pol 2016;87:659-63.
4. Azim HA Jr., Partridge AH. Biology of breast cancer in young women. Breast Cancer Res 2014;16:427.
5. Kolak A, Kamińska M, Sygit K, Budny A, Surdyka D, Kukiełka-Budny B, *et al.* Primary and secondary prevention of breast cancer. Ann Agric Environ Med 2017;24:549-53.
6. Kim KJ, Huh SJ, Yang JH, Park W, Nam SJ, Kim JH, *et al.* Treatment results and prognostic factors of early breast cancer treated with a breast conserving operation and radiotherapy. Jpn J Clin Oncol 2005;35:126-33.
7. Invasive Breast Cancer (IDC/ILC), American Cancer Society; 2023. Available from: https://www.cancer.org/cancer/breast-cancer/about/types-of-breast-cancer/invasive-breast-cancer.html. [Last accessed 2021 Nov 19].
8. McCart Reed AE, Kutasovic JR, Lakhani SR, Simpson PT. Invasive lobular carcinoma of the breast: Morphology, biomarkers and 'omics. Breast Cancer Res 2015;17:12.
9. Li CI, Anderson BO, Daling JR, Moe RE. Trends in incidence rates of invasive lobular and ductal breast carcinoma. JAMA 2003;289:1421-4.
10. Lee JH, Park S, Park HS, Park BW. Clinicopathological features of infiltrating lobular carcinomas comparing with infiltrating ductal carcinomas: A case control study. World J Surg Oncol 2010;8:34.
11. Orvieto E, Maiorano E, Bottiglieri L, Maisonneuve P, Rotmensz N, Galimberti V, *et al.* Clinicopathologic characteristics of invasive lobular carcinoma of the breast: Results of an analysis of 530 cases from a single institution. Cancer 2008;113:1511-20.

12. Arpino G, Bardou VJ, Clark GM, Elledge RM. Infiltrating lobular carcinoma of the breast: Tumor characteristics and clinical outcome. Breast Cancer Res 2004;6:R149-56.
13. Mersin H, Yildirim E, Gülben K, Berberoğlu U. Is invasive lobular carcinoma different from invasive ductal carcinoma? Eur J Surg Oncol 2003;29:390-5.
14. Sastre-Garau X, Jouve M, Asselain B, Vincent-Salomon A, Beuzeboc P, Dorval T, *et al.* Infiltrating lobular carcinoma of the breast. Clinicopathologic analysis of 975 cases with reference to data on conservative therapy and metastatic patterns. Cancer 1996;77:113-20.
15. Mathew A, Rajagopal PS, Villgran V, Sandhu GS, Jankowitz RC, Jacob M, *et al.* Distinct pattern of metastases in patients with invasive lobular carcinoma of the breast. Geburtshilfe Frauenheilkd 2017;77:660-6.
16. Korhonen T, Kuukasjärvi T, Huhtala H, Alarmo EL, Holli K, Kallioniemi A, *et al.* The impact of lobular and ductal breast cancer histology on the metastatic behavior and long term survival of breast cancer patients. Breast 2013;22:1119-24.
17. Inoue M, Nakagomi H, Nakada H, Furuya K, Ikegame K, Watanabe H, *et al.* Specific sites of metastases in invasive lobular carcinoma: A retrospective cohort study of metastatic breast cancer. Breast Cancer 2017;24:667-72.
18. Maughan KL, Lutterbie MA, Ham PS. Treatment of breast cancer. Am Fam Physician 2010;81:1339-46.
19. Shamsi M, Pirayesh Islamian J. Breast cancer: Early diagnosis and effective treatment by drug delivery tracing. Nucl Med Rev Cent East Eur 2017;20:45-8.
20. Arriagada R, Le MG, Dunant A, Tubiana M, Contesso G. Twenty-five years of follow-up in patients with operable breast carcinoma: Correlation between clinicopathologic factors and the risk of death in each 5-year period. Cancer 2006;106:743-50.
21. Heusner TA, Kuemmel S, Hahn S, Koeninger A, Otterbach F, Hamami ME, *et al*. Diagnostic value of full-dose FDG PET/CT for axillary lymph node staging in breast cancer patients. Eur J Nucl Med Mol Imaging 2009;36:1543-50.
22. Riegger C, Koeninger A, Hartung V, Otterbach F, Kimmig R, Forsting M, *et al.* Comparison of the diagnostic value of FDG-PET/CT and axillary ultrasound for the detection of lymph node metastases in breast cancer patients. Acta Radiol 2012;53:1092-8.
23. Liang X, Yu J, Wen B, Xie J, Cai Q, Yang Q. MRI and FDG-PET/CT based assessment of axillary lymph node metastasis in early breast cancer: A meta-analysis. Clin Radiol 2017;72:295-301.
24. Song BI, Kim HW, Won KS. Predictive value of (18) F-FDG PET/CT for axillary lymph node metastasis in invasive ductal breast cancer. Ann Surg Oncol 2017;24:2174-81.
25. Peare R, Staff RT, Heys SD. The use of FDG-PET in assessing axillary lymph node status in breast cancer: A systematic review and meta-analysis of the literature. Breast Cancer Res Treat 2010;123:281-90.
26. Robertson IJ, Hand F, Kell MR. FDG-PET/CT in the staging of local/regional metastases in breast cancer. Breast 2011;20:491-4.
27. Litjens G, Kooi T, Bejnordi BE, Setio AA, Ciompi F, Ghafoorian M, *et al*. A survey on deep learning in medical image analysis. Med Image Anal 2017;42:60-88.
28. Wang H, Zhou Z, Li Y, Chen Z, Lu P, Wang W, *et al.* Comparison of machine learning methods for classifying mediastinal lymph node metastasis of non-small cell lung cancer from (18) F-FDG PET/CT images. EJNMMI Res 2017;7:11.
29. Groheux D, Hindie E. Breast cancer: Initial workup and staging with FDG PET/CT. Clin Transl Imaging 2021;9:221-31.
30. Manohar K, Mittal BR, Senthil R, Kashyap R, Bhattacharya A, Singh G. Clinical utility of F-18 FDG PET/CT in recurrent breast carcinoma. Nucl Med Commun 2012;33:591-6.
31. Gajjala SR, Hulikal N, Kadiyala S, Kottu R, Kalawat T. Whole-body (18) F-fluorodeoxyglucose positron emission tomography-computed tomography ((18) F-FDG PET/CT) for staging locally advanced breast cancer: A prospective study from a tertiary cancer centre in South India. Indian J Med Res 2018;147:256-62.
32. Patel MM, Le-Petross HT. Baseline FDG PET-CT imaging is necessary for newly diagnosed inflammatory breast cancer patients: A narrative review. Chin Clin Oncol 2021;10:56.
33. Hadad ZS, Afzelius P, Sørensen SM, Jurik AG. Clinical relevance of 18F-FDG-PET/CT incidental findings. Dan Med J 2020;67:A10190553.
34. Agress H Jr., Cooper BZ. Detection of clinically unexpected malignant and premalignant tumors with whole-body FDG PET: Histopathologic comparison. Radiology 2004;230:417-22.
35. Ozkol V, Alper E, Aydin N, Ozkol HF, Topal NB, Akpinar AT. The clinical value of incidental 18F-fluorodeoxyglucose-avid foci detected on positron emission tomography/computed tomography. Nucl Med Commun 2010;31:128-36.
36. Luo Y, Li J, Huang L, Han Y, Tian X, Ma W, *et al.* Value of dynamic metabolic curves and artificial neural network prediction models based on 18F-FDG PET/CT multiphase imaging in differentiating nonspecific solitary pulmonary lesions: A pilot study. Nucl Med Commun 2022;43:1204-16.
37. Marschner SN, Lombardo E, Minibek L, Holzgreve A, Kaiser L, Albert NL, *et al.* Risk stratification using (18) F-FDG PET/CT and artificial neural networks in head and neck cancer patients undergoing radiotherapy. Diagnostics (Basel) 2021;11:1581.
38. Wallis D, Soussan M, Lacroix M, Akl P, Duboucher C, Buvat I. An [18F] FDG-PET/CT deep learning method for fully automated detection of pathological mediastinal lymph nodes in lung cancer patients. Eur J Nucl Med Mol Imaging 2022;49:881-8.
39. Hirata K, Kobayashi K, Wong KP, Manabe O, Surmak A, Tamaki N, *et al*. A semi-automated technique determining the liver standardized uptake value reference for tumor delineation in FDG PET-CT. PLoS One 2014;9:e105682.
40. Palaz D, Doss MM, Collobert R. Convolutional neural networks-based continuous speech recognition using raw speech signal. In: 2015 IEEE International Conference on Acoustics, Speech and Signal Processing (ICASSP). Switzerland: IEEE; 2015. p. 4295-9.
41. Luo Y, Wong Y, Kankanhalli M, Zhao Q. G -softmax: Improving intraclass compactness and interclass separability of features. IEEE Trans Neural Netw Learn Syst 2020;31:685-99.
42. Abdel-Hamid O, Rahman MA, Jiang H, Deng L, Penn G, Yu D. Convolutional neural networks for speech recognition. IEEE/ACM Trans Audio Speech Lang Process 2014;22:1533-45.
43. Moons KG, Altman DG, Reitsma JB, Ioannidis JP, Macaskill P, Steyerberg EW, *et al*. Transparent reporting of a multivariable prediction model for individual prognosis or diagnosis (TRIPOD): Explanation and elaboration. Ann Intern Med 2015;162:W1-73.
44. Caresia Aroztegui AP, García Vicente AM, Alvarez Ruiz S, Delgado Bolton RC, Orcajo Rincon J, Garcia Garzon JR, *et al.* 18F-FDG PET/CT in breast cancer: Evidence-based recommendations in initial staging. Tumour Biol 2017;39:1010428317728285.
45. Groheux D, Cochet A, Humbert O, Alberini JL, Hindié E, Mankoff D. ^{18}F-FDG PET/CT for staging and restaging of breast cancer. J Nucl Med 2016;57 Suppl 1:17-26S.
46. Paydary K, Seraj SM, Zadeh MZ, Emamzadehfard S, Shamchi SP, Gholami S, *et al.* The evolving role of FDG-PET/CT in the diagnosis, staging, and treatment of breast cancer. Mol Imaging Biol 2019;21:1-10.
47. Groheux D, Mankoff D, Espié M, Hindié E. ^{18}F-FDG PET/CT in the early prediction of pathological response in aggressive subtypes of breast cancer: Review of the literature and recommendations for use in clinical trials. Eur J Nucl Med Mol Imaging 2016;43:983-93.
48. Usmani S, Albader FL, Marafi F, Elhaggracy RS. Primary breast lymphoma mimicking metastatic breast cancer on 18F-FDG PET-CT. J Pak Med Assoc 2022;72:1241-2.
49. Taralli S, Scolozzi V, Boldrini L, Lenkowicz J, Pelliccioni A, Lorusso M, *et al.* Application of artificial neural network to preoperative (18) F-FDG PET/CT for predicting pathological nodal involvement in non-small-cell lung cancer patients. Front Med (Lausanne) 2021;8:664529.
50. Li Z, Kitajima K, Hirata K, Togo R, Takenaka J, Miyoshi Y, *et al.* Preliminary study of AI-assisted diagnosis using FDG-PET/CT for axillary lymph node metastasis in patients with breast cancer. EJNMMI Res 2021;11:10.

51. Inaki A, Nakajima K, Wakabayashi H, Mochizuki T, Kinuya S. Fully automated analysis for bone scintigraphy with artificial neural network: Usefulness of bone scan index (BSI) in breast cancer. Ann Nucl Med 2019;33:755-65.
52. Leal JP, Rowe SP, Stearns V, Connolly RM, Vaklavas C, Liu MC, *et al.* Automated lesion detection of breast cancer in [(18) F] FDG PET/CT using a novel AI-based workflow. Front Oncol 2022;12:1007874.
53. Dihge L, Ohlsson M, Edén P, Bendahl PO, Rydén L. Artificial neural network models to predict nodal status in clinically node-negative breast cancer. BMC Cancer 2019;19:610.
54. Sepandi M, Taghdir M, Rezaianzadeh A, Rahimikazerooni S. Assessing breast cancer risk with an artificial neural network. Asian Pac J Cancer Prev 2018;19:1017-9.
55. Chai Q, Mei L, Zou Z, Peng H. Value of artificial neural network ultrasound in improving breast cancer diagnosis. Comput Intell Neurosci 2022;2022:1779337.
56. Mehdy MM, Ng PY, Shair EF, Saleh NI, Gomes C. Artificial neural networks in image processing for early detection of breast cancer. Comput Math Methods Med 2017;2017:2610628.
57. Jia D, Chen C, Chen C, Chen F, Zhang N, Yan Z, *et al.* Breast cancer case identification based on deep learning and bioinformatics analysis. Front Genet 2021;12:628136.
58. Ren T, Lin S, Huang P, Duong TQ. Convolutional neural network of multiparametric MRI accurately detects axillary lymph node metastasis in breast cancer patients with pre neoadjuvant chemotherapy. Clin Breast Cancer 2022;22:170-7.

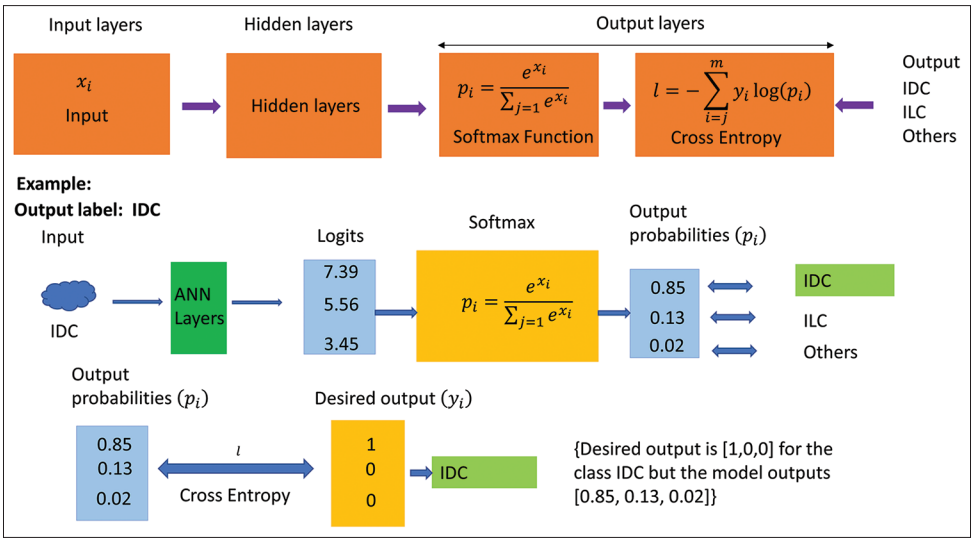

Supplemental Figure 1: Based on the output label invasive ductal cancer, the artificial neural network's output values are calculated using the cross-entropy and Softmax functions in the output layers. ILC: Invasive lobular cancer, IDC: Invasive ductal cancer, ANN: Artificial neural network

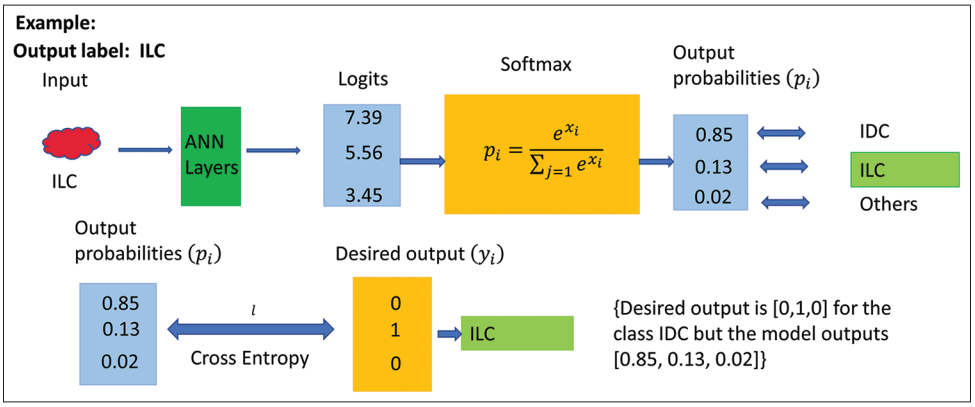

Supplemental Figure 2: Based on the output label, invasive lobular cancer, the artificial neural network's output values in the output layers use the cross-entropy and Softmax functions. ILC: Invasive lobular cancer, IDC: Invasive ductal cancer, ANN: Artificial neural network

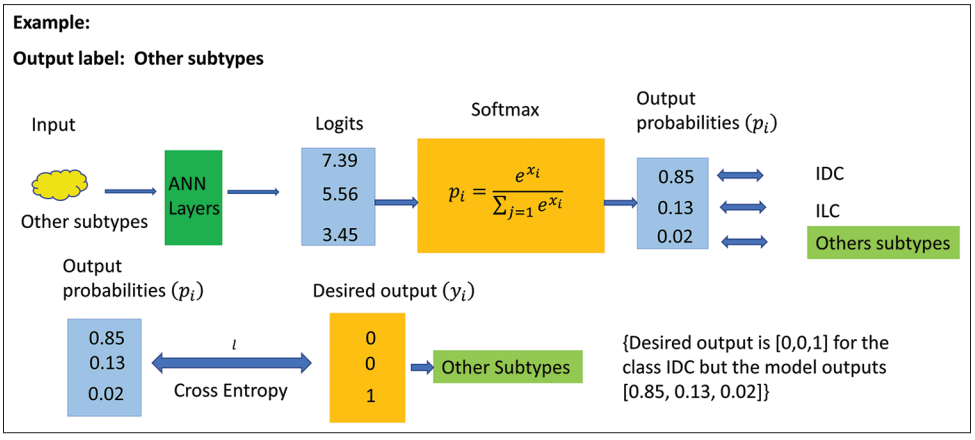

Supplemental Figure 3: Based on the output label and other subtypes, the artificial neural network's output values are determined by utilizing the cross-entropy and Softmax functions in the output layers. ILC: Invasive lobular cancer, IDC: Invasive ductal cancer, ANN: Artificial neural network

Supplemental Table 1: An overview of the stratified cross-validation artificial neural network model	
Correctly classified instances, *n* (%)	136 (95.77)
Incorrectly classified instances, *n* (%)	6 (4.23)
Kappa statistic	0.8424
Mean absolute error	0.0533
Root mean squared error	0.1711
Relative absolute error (%)	27.27
Root relative squared error (%)	55.54
Total number of instances	142